RSC Advances

ROYAL SOCIETY OF CHEMISTRY

www.rsc.org/advances

A LIGHT HARVESTING MONONUCLEAR MANGANESE (II) COMPLEX: SYNTHESIS, CHARACTERIZATION, DFT CALCULATIONS AND PHOTOPHYSICAL PROFILE

Debalina Ghosh, Urmila Saha and Kalyan K. Mukherjea

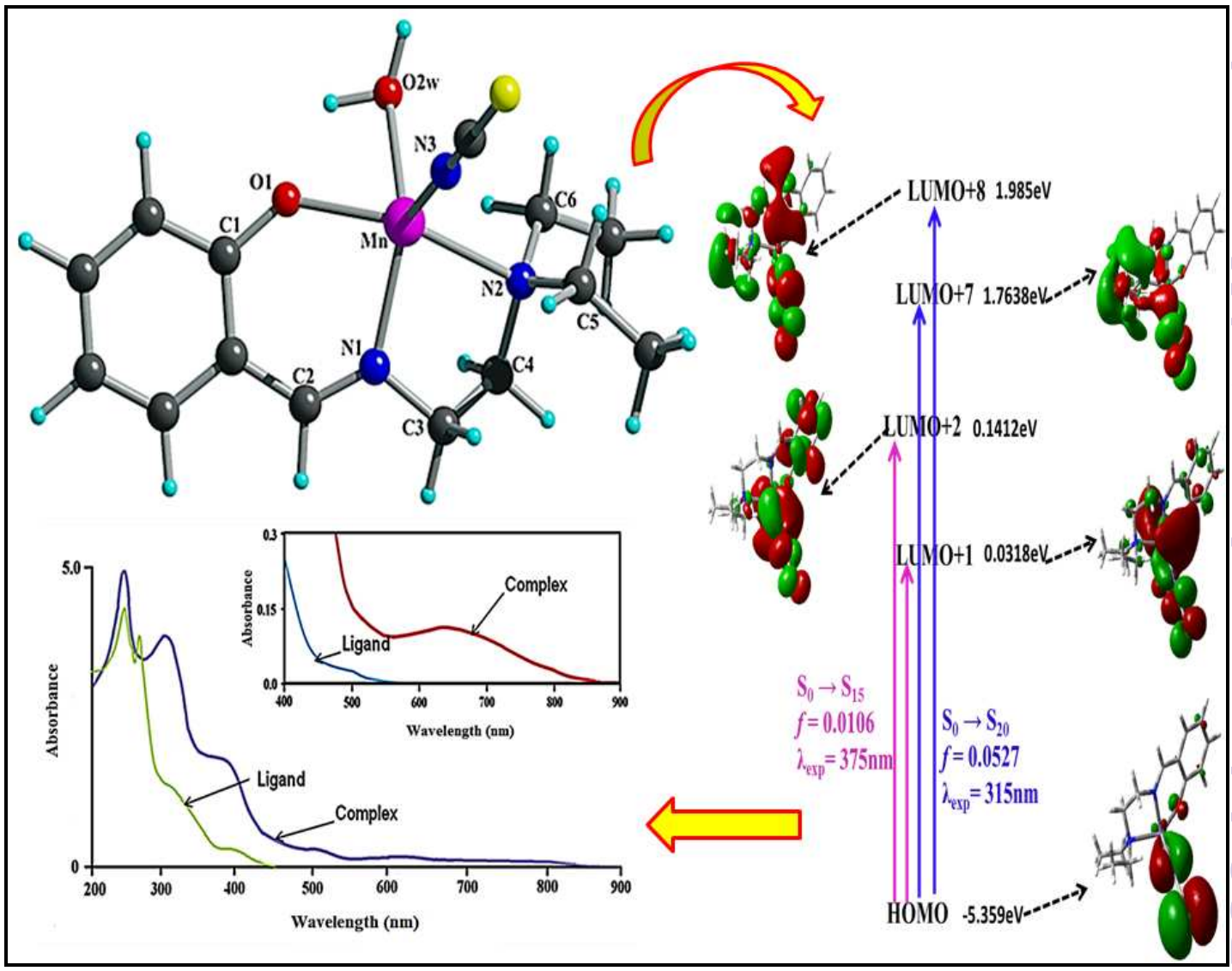

A Light Harvesting Mononuclear Manganese (II) Complex: Synthesis, Characterization, DFT and TDDFT Calculations and Photophysical Profile

Debalina Ghosh, Urmila Saha and Kalyan K. Mukherjea*,

*Author for correspondence:

Department of Chemistry, Jadavpur University, Calcutta (Kolkata) - 700032, India.

E-mail: k_mukherjea@yahoo.com; Fax: +91-33-2414-6584; Tel: +91-9831129321

A new Manganese (II) [Mn^{II}(DEMP)(NCS)(H_2O)] (DEMP = Schiff base derived from salicylaldehyde and 2-Diethylaminoethylamine) complex has been synthesized and characterized by ESI-mass, IR, UV-vis, ^{1}H and ^{13}C NMR, EPR and thermo gravimetric analysis. The structure of the complex has been optimized by DFT and TDDFT calculations. The complex has been found to exhibit strong fluorescence emission in different solvents of various polarities which is characterized by longer lifetimes in more polar solvents, accompanied with reasonably good quantum yield. The complex is capable of absorbing light ranging from 200-850 nm. Thus, the molecule contains the light harvesting components that can harvest the entire range of sunlight falling on earth.

Introduction

Manganese is an important metal in biological system. It is essential for all forms of life. It accumulates in mitochondria where it is essentially required. Manganese plays an obligatory role in many cellular processes including lipid, protein and carbohydrate metabolism and is used as a cofactor by a diverse array of enzymes.[1-2] The element is an essential trace mineral for all known living organisms. Manganese (Mn) is required for the growth and survival of most, if not all, living organisms. Until recently, relatively little was known about how bacteria take up trace nutrients such as manganese, nickel, copper and zinc, or how they regulate intracellular levels of these metal ions in response to availability and demand. Several metalloenzymes of manganese are known, such as arginase, pyruvate carboxylase and superoxide dismutase. Manganese enzymes are essential particularly in the detoxification of superoxide free radicals in micro-organisms[3-9] and decomposition of O_2^- radical, using superoxide dismutase. For years together, it has been known that oxygen evolving photosynthetic organisms have a requirement for manganese.[10-11] Depletion of manganese in plants or algae by withholding it from the growth medium leads to the loss of O_2 evolution capability.[12] Various experiments point to a site on the donor side of photosystem II as the location for the manganese.[13-16] To date, it has not been possible to detect directly the Mn-containing entity that is responsible for mediating O_2 evolution. It can be concluded that, the most primordial example of biological importance of manganese, is the photo-induced oxidation of water to molecular oxygen in photosystem II (PS II) of green plants.[17-22] Manganese is believed to be an essential component, in this regard. The photo-activation of manganese complexes is now of interest not only for modelling of PS II, but also for the development of new photo active-materials.[23-31] The photosynthetic manganese catalyzed reaction in PS II is solely dependent on the light harvesting process. Nature has deployed a number of pigments to harvest the entire range of sunlight falling on earth. Artificial photosynthesis is an area of active research which, as an integral part, requires light harvesting components. So, scientists are active to explore the possibility of developing artificial light harvesting compounds.[32-38] The effective light harvesting compounds should have the ability to absorb light of a wide range of wavelengths to

be as close as possible to the natural photosynthetic light harvesting pigments. In the present project, attempt has been made to develop a light harvesting mononuclear manganese complex. The complex has been synthesized and characterized spectroscopically. The structure of the complex has been optimized with theoretical DFT calculations and detailed photophysical properties have been examined for its exploitation as a possible light harvesting agent as it is capable of harvesting light of the entire visible region i.e. the entire region of the sunlight falling on earth.

Results and discussion

Characterization of the ligand

ESI-mass spectra of the ligand. The ESI-mass spectra of the ligand show a peak of the protonataed product of the ligand at 221.16 with 100% abundance (S3 (b)).

Therefore the ligand can be formulated as $C_{13}H_{20}N_2O$.

IR characterization of the ligand. The free Schiff base shows the characteristic azomethine ($\nu_{C=N}$) and OH group frequencies at around 1621 cm^{-1} and 3418 cm^{-1} respectively.

^{1}H NMR spectra of the ligand. The signals recorded at 7.46–6.78 ppm in the ligand spectrum are due to the presence of four aromatic protons in DEMP while the signal at 8.61 appears for the presence of the –OH group in aromatic ring of the ligand.

Characterization of the complex

ESI-mass spectra of the complex. The ESI-mass spectra of the complex show the mass of the complex added with a sodium at 373.11 with maximum abundance (S4).

Thermo gravimetric analysis. The presence of the coordinated water in the complex is characterized by a mass loss above 120°C. The ~35% mass loss occurred up to 225°C is a combined effect of the elimination of coordinated water, SCN and a part of the Schiff base.[39]

Therefore the molecular formula of the compound is $MnC_{14}H_{22}N_3O_2S$.

IR characterization of the complex. Some important infrared absorption frequencies of the ligand and metal complex are analysed. The azomethine and OH group frequencies of free Schiff base shifts towards the lower frequency region in the spectra of the complex at around 1618 cm^{-1} due to involvement of the N atom of the –C=N- group[40-43] in coordination, whereas the ν_{OH} band shifts to 3172 cm^{-1} suggesting the engagement of this group in coordination with the metal centre. The band at 3386 cm^{-1} in the complex arises due to the vibration of metal oxygen bond of the axially coordinated water molecule ($\nu_{Mn(1)-O(2)}$). The bands at 1598.8, 983.85, 1095.93 cm^{-1} are due to $\nu_{Mn-N(11)}$, $\nu_{Mn-N(14)}$ and $\nu_{Mn-O(3)}$ vibrations respectively of the coordinated Schiff base (S2.). Infrared bands due to NCS groups, ν_{CN} 2054 cm^{-1}, ν_{CS} 800 cm^{-1} are consistent with terminally N-bonded NCS groups in the complex.[44-45]

^{1}H NMR spectra of complex. The signal observed at 8.61 ppm in the DEMP ligand has disappeared in the complex, as a result of the deprotonation of the –OH group during coordination. The multiple proton signals appearing at 7.46-6.78 ppm in DEMP, due to the presence of the aromatic protons are shifted to 7.40-6.33 ppm in the complex. The above ^{1}H NMR spectral results clearly indicates that the ligand DEMP is coordinated with the metal in the present complex.

Magnetic moment. The room temperature (298K) magnetic moment of the complex is found to be 5.88 B.M. which indicates the presence of Mn(II) centre in the complex.[46]

EPR spectroscopy. The EPR spectrum of complex [Mn^{II} (DEMP)(NCS)(H_2O)] was recorded in the solid state at room temperature. A single EPR line is observed (Figure 1), which reveals the presence of a strong signal in the g = 1.95 region. Such one-line spectrum devoid of any hyperfine structure suggests unequivocally the mononuclear nature of the complex.[47]

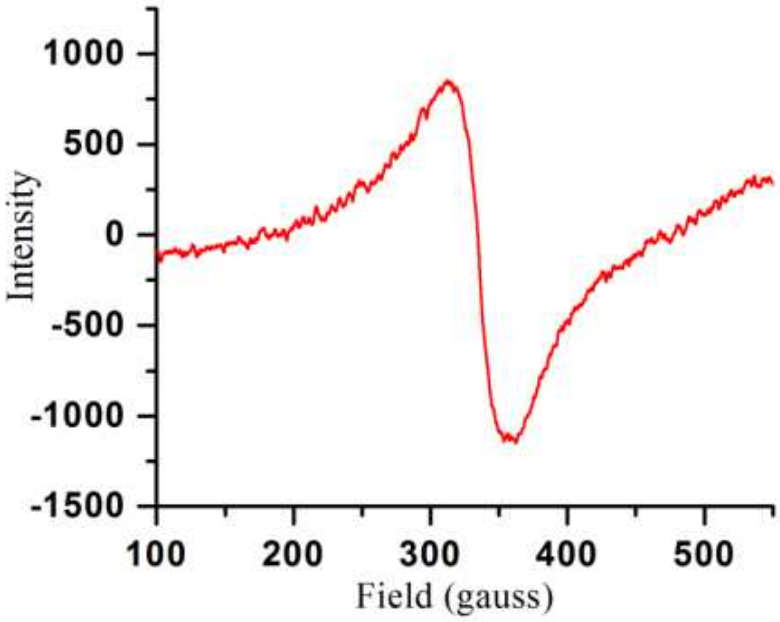

Figure 1: EPR spectra of complex at 298 K. (freq. = 9445.141 MHz, power = 0.9908 mW, sweep time = 4.00 min.)

UV–vis spectrophotometric study. The electronic spectrum of the ligand, shows band at 253 nm (ε = 6015 M^{-1} cm^{-1}) attributed to benzene π→π* transition, and the band at 312 nm (ε = 2108 M^{-1} cm^{-1}) is assigned to the imino n→π* transition. The broad peak at around 375 nm (ε = 2728 M^{-1} cm^{-1}) in the complex is assignable to the ligand to metal charge transfer transition. Another peak at 251 nm (ε =7300 M^{-1} cm^{-1})[43-45] arises due to the intraligand charge transfer transition (Figure 2a). The very important aspect of this work is the appearance of a continuous absorption of the metal complex ranging from 200 nm to 850 nm in methanol solution (Figure 2a)**.** This absorption allows the metal complex to cover almost entirely the sunlight falling on earth. To understand the effect of the polarity of the medium, the absorption spectra of ligand and its complex were recorded in acetonitrile, DMF, MeOH, DMSO, chloroform, DCM, THF (Figure 2b, 2c). The spectra show a continuous decrease of intensity as well as red shift with decreasing polarity of the solvents (Table 1). In presence of polar solvent molecules, the electronic transition in case of the ligand being so rapid with increasing polarity of the solvent molecules, that the spectral transition has become more feasible due to lower energy gap, i.e. there occurs bathochromic or red shift in ligand with the higher polarity of the solvents.

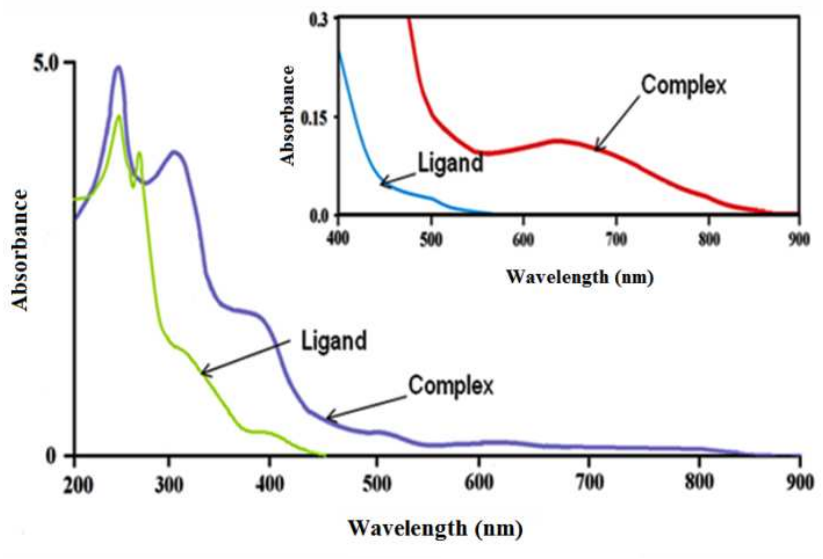

(a)

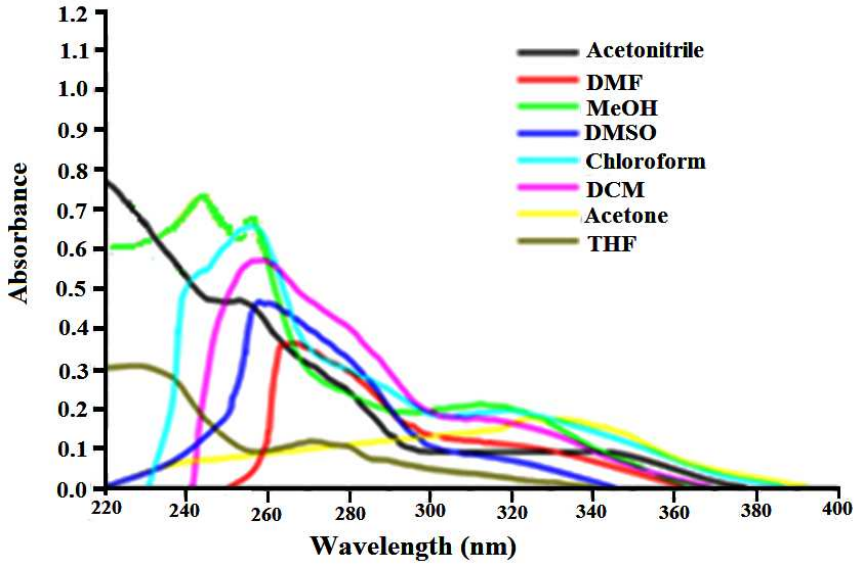

(b)

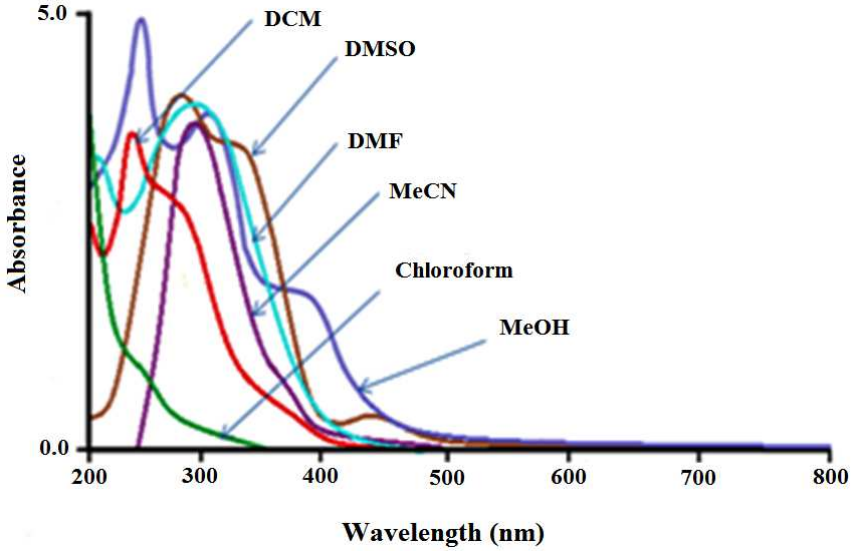

(c)

Figure 2: Electronic spectra in methanol at 6.45×10^{-4} M of both ligand and complex (a) and the amplified visible absorption of the methanolic solutions of ligand and the complex (inset). Absorbance spectra of 10^{-4} (M) ligand (b) and metal complex (c) in various solvents,

Table 1: Absorption λ_{max} (nm) of complex and ligand in different solvents

SOLVENT	(complex) λ_{max} (nm) 10^{-4} (M)	(ligand) λ_{max} (nm) 10^{-4} (M)
DMSO	263	258
DMF	269	266
Acetonitrile	288	254
MeOH	254	253
Acetone	325	333
DCM	299	259
THF	289	269
$CHCl_3$	305	256

Optimization of molecular geometry and electronic structure. DFT study has been proved to be an important tool to obtain better insights into the geometry, electronic structure, and optical properties of these systems. The geometry of both the ligand and the metal complex has been optimized by using Density Functional Theory (DFT). The optimized geometry of HL (DEMP) and its Mn^{2+} complex is shown in Figure 3a and 3b respectively. Both HL and Mn^{2+} complex had C1 point group. For both the ligand and complex, we are able to optimize only the ground state geometries. Main optimized geometrical parameters of the complex are listed in Table 1 and the optimized structure of DEMP and complex are given in Figure 3. The geometry of the penta-coordinated metal centre can be measured by the Addison parameter (τ), which is 0.1512, 0.1991, 0.0969 in 6-31G, 6-311G and 6-31++G(d,p) under B3LYP respectively for complex, [$\tau = (\alpha - \beta)/60$, where α and β are the two largest Ligand-Metal-Ligand angles of the coordination sphere],

suggesting a slightly distorted square pyramidal geometry ($\tau = 0$ for a perfect square pyramid and $\tau = 1$ for a perfect trigonal bipyramid). Hence, the modelled geometry possess a distorted square pyramidal arrangement around the Mn(II) centre. A comparison of the results of the theoretical calculations undertaken by different basis sets ([6-31G, 6-311G and 6-31++G(d,p)] under B3LYP) show that the variations in structural parameters are negligibly small (Figure 3, Table 1). The calculated IR stretching frequencies of the complex are compared with experimental findings (Table-S2). Hence, all the DFT calculations unequivocally support the structure of the Mn compound. In complex all calculated Mn-N distances occur in the range 2.005-2.428 Å and Mn-O distances are in the range 2.083-2.259 Å. On complexation, some C-N and C-O bond lengths are changed with respect to that in free ligand and Table 2 describes the change in bond lengths in complex compared to free ligand.

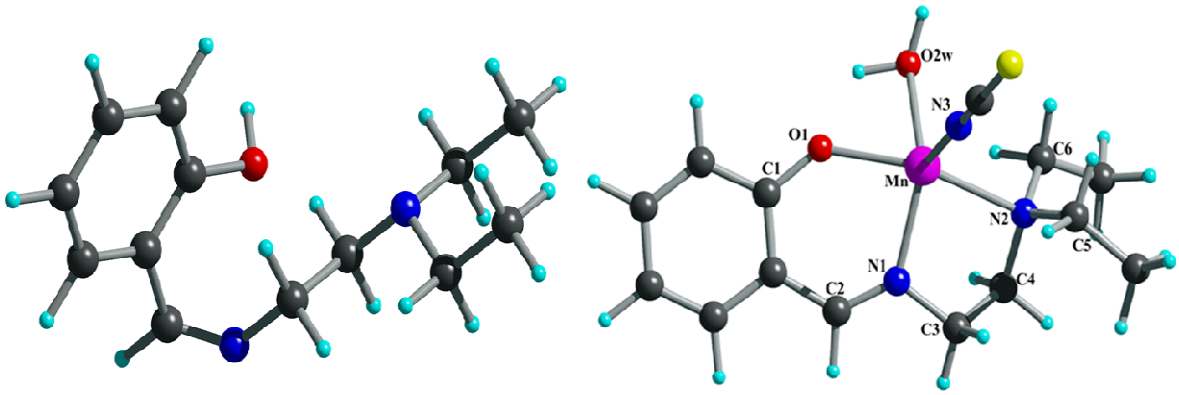

(a) (b)

Figure 3: Optimized geometry of (a) ligand (DEMP) and (b) Complex Mn(DEMP)(NCS)(H_2O).

Table 1: Selected optimized geometrical parameters for **1** in the ground state calculated at B3LYP Levels.

Bond Length(Å)	**6-31G**	**6-311G**	**6-31++G**
Mn-N1	2.150	2.162	2.151
Mn-N2	2.408	2.387	2.428
Mn-N3	2.007	2.012	2.005
Mn-O1	2.088	2.089	2.083
Mn-O2w	2.231	2.226	2.259
Bond Angles (^{o})			
N1-Mn-N2	78.223	78.258	77.893
N2-Mn-N3	101.560	96.239	101.489
N3-Mn-O2w	103.002	99.275	102.249
O1-Mn-O2w	69.379	70.533	69.910
O1-Mn-N1	83.508	83.530	83.861
O1-Mn-N2	141.408	150.703	140.391
N1-Mn-N3	124.351	138.712	122.928
N2-Mn-O2w	98.996	100.157	99.077
O1-Mn-N3	116.775	112.477	117.893
N1-Mn-O2w	132.336	122.010	134.574

Table 3: Change in bond lengths in the complex compared to free ligand in the ground state calculated at B3LYP/6-31G Levels.

	Bond Lengths (Å)	
	Free ligand (DEMP)	Complex
O1-C1	1.388	1.330
N1-C2	1.277	1.307
N1-C3	1.480	1.472
N2-C4	1.479	1.492
N2-C5	1.491	1.509
N2-C6	1.481	1.501

In case of DEMP at ground state, the electron density at HOMO – 2, LUMO and LUMO + 1 orbitals mainly resides on the benzene moiety while a considerable contribution comes from 2-diethylaminoethylamine moiety along with the contribution of benzene moiety in HOMO – 1 and HOMO orbitals. The energy difference between HOMO and LUMO is 4.34 eV of ligand (DEMP). In case of the complex all the LUMO+2, LUMO+7and LUMO+8 orbitals are mainly originating from ligand π and π* orbital contributions while the HOMO and LUMO+1 orbitals arise from the contribution of metal d orbitals along with ligand π orbital. The energy difference between HOMO and LUMO is 3.48 eV in the complex.These compositions are useful in understanding the nature of transition as well as the absorption spectra of both the ligand and complex (vide infra).

The ligand shows two absorption bands at 310 and 253 nm in methanolic solution at room temperature and both have ILCT character. This assignment was supported by TDDFT calculations. These two absorption bands can be assigned to the $S_0 \rightarrow S_1$ and $S_0 \rightarrow S_6$ transitions. The absorption energies

along with their oscillator strengths, the main configurations and their assignments were calculated using TDDFT method and the related data are given in Table 4.

The complex shows two absorption bands at 375 and 315 nm in methanolic solution at room temperature. The absorptions calculated from TDDFT show bands 379 and 333 nm for the complex (Figure 4). This calculated value is in excellent agreement with the experimental results. These two absorption bands can be assigned to the $S_0 \rightarrow S_{15}$ and $S_0 \rightarrow S_{20}$ transitions, respectively and both the transitions originate from an admixture of MLCT and ILCT transitions (Table 5).

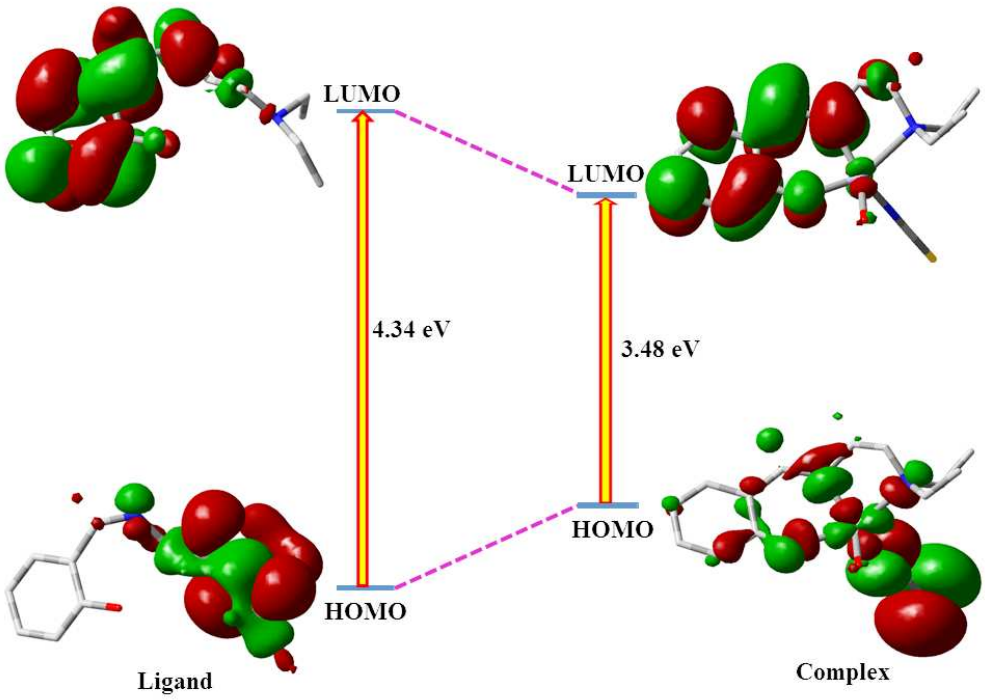

Figure 5: Frontier molecular orbital of ccomplex as well as ligand optimized

Table 4 Selected Parameters for the vertical excitation (UV-vis absorptions) of DEMP; electronic excitation energies (eV) and oscillator strengths (f), configurations of the low-lying excited states of DEMP; calculation of the S_0-S_1 energy gaps based on optimized ground-state geometries (UV-vis absorption) (CH_3OH used as solvent).

Electronic transition	**Composition**	**Excitation energy**	**Oscillator strength (f)**	**CI**	**Assign**	**λ_{theo} (nm)**	**λ_{exp} (nm)**
S0 → S1	HOMO–2 →LUMO HOMO → LUMO	3.9974 eV (310 nm)	0.1413	0.32108 0.62216	ILCT ILCT	310	312
S0 → S6	HOMO–2→ LUMO + 1 HOMO–1→ LUMO + 1	4.8968 eV (253 nm)	0.0851	4.8968 0.25357	ILCT ILCT	253	253

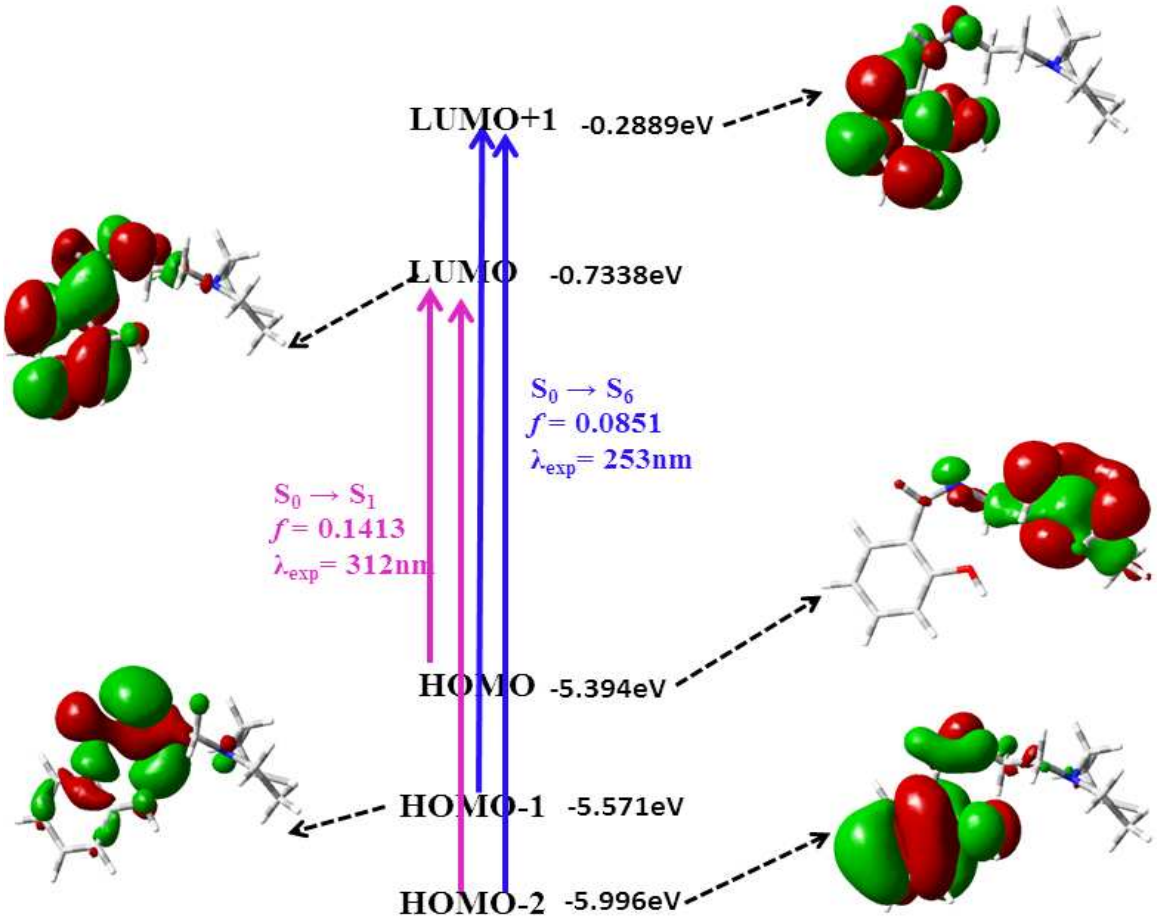

Figure 6: Frontier molecular orbitals involved in the UV-vis absorption of ligand (DEMP).

Table 5. Main calculated optical transition for the complex with composition in terms of molecular orbital contribution of the transition, vertical excitation energies, and oscillator strength in methanol.

Electronic transition	**Composition**	**Excitation energy**	**Oscillator strength (*f*)**	**CI**	**Transition assigned**	**λ_{theo} (nm)**	**λ_{exp} (nm)**
$S_0 \rightarrow S_{15}$	HOMO–2 →LUMO+5 HOMO–3 → LUMO+5 HOMO → LUMO + 2 HOMO → LUMO + 1	3.2691eV (379 nm)	0.0106	-0.11382 -0.14107 0.89978 -0.14828	ILCT ILCT MLCT/ILCT MLCT/ILCT	379	375
$S_0 \rightarrow S_{20}$	HOMO → LUMO + 7 HOMO → LUMO + 8	3.7183eV (333 nm)	0.0527	-0.23910 0.95162	MLCT/ILCT MLCT/ILCT	333	315

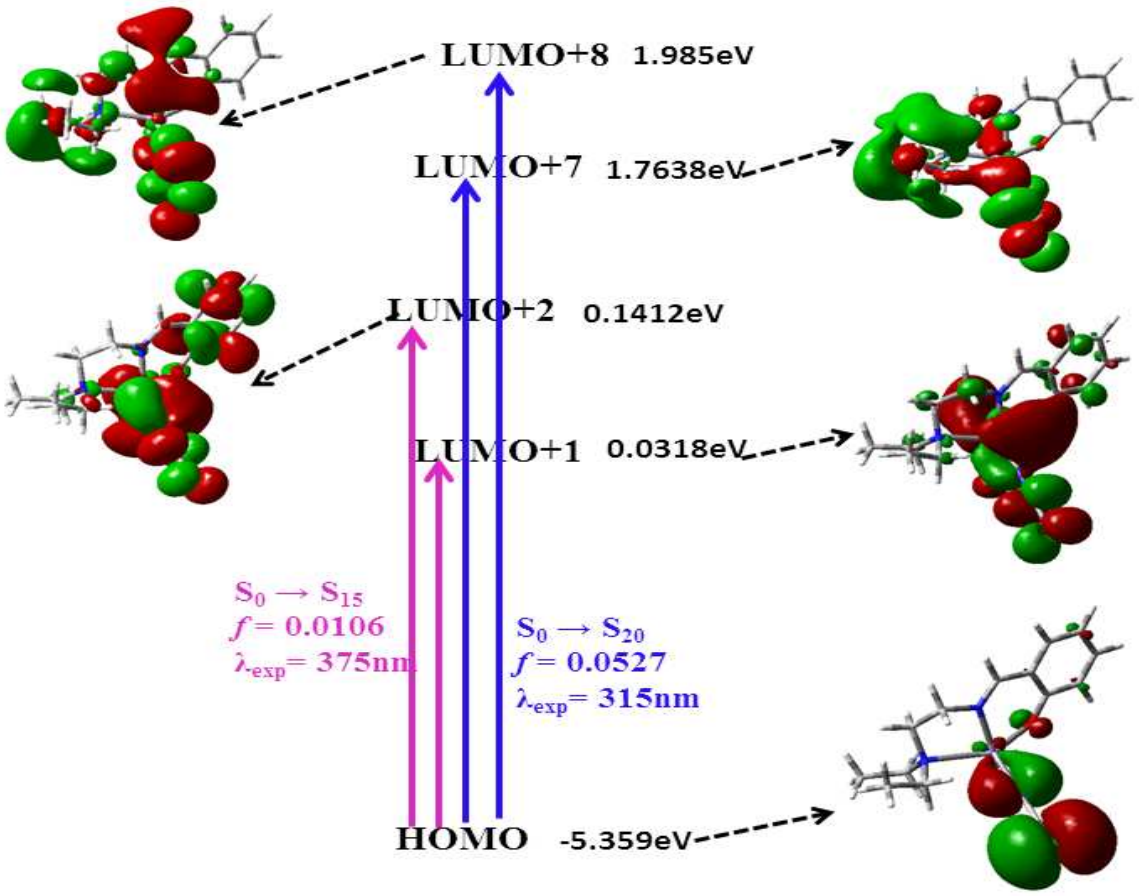

Figure 7: Frontier molecular orbitals involved in the UV-vis absorption of metal complex.

Photophysical activity of the complex. The main focus of the study is the development of the light harvesting metal based compound. The light harvesting property is characterized by the photophysical profile of any photophore. So, the photophysical profile of the [Mn^{II}(DEMP)(NCS)(H_2O)] compound has been investigated by fluorescence spectroscopy. The emission spectra of both the ligand and the complex were studied in varied solution concentrations and at different solvent polarity.

The Fluorescence emission spectra of 10^{-4}, 10^{-5} and 10^{-6} M ligand solutions of 2-[(2-Diethylamino ethylimino)-methyl]-phenol impart different fluorescence intensities (S1 (a)) with same shape of spectra, and the effect of the polarity of solvent on the ligand also show similar patterns, except for THF, in which

the emission spectrum does not split but show almost one sharp emission, with the highest fluorescence intensity (Figure 7(a)).

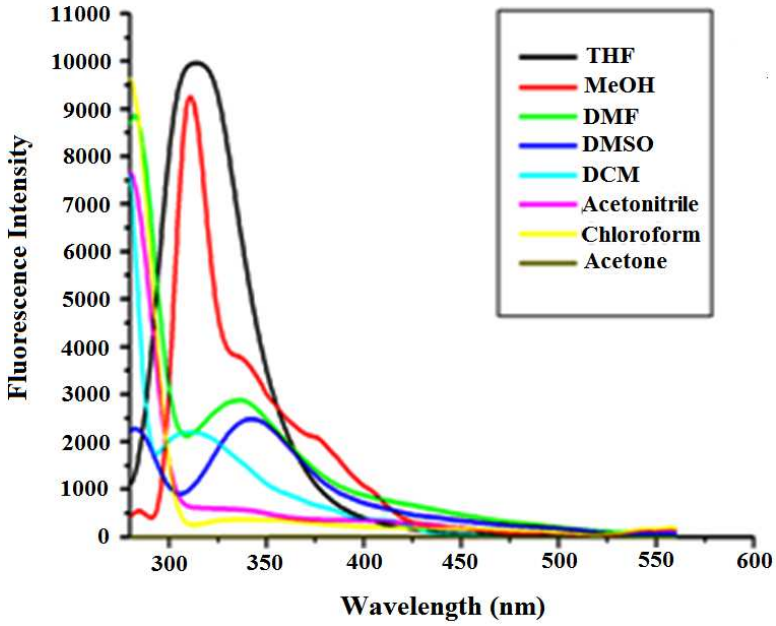

(a)

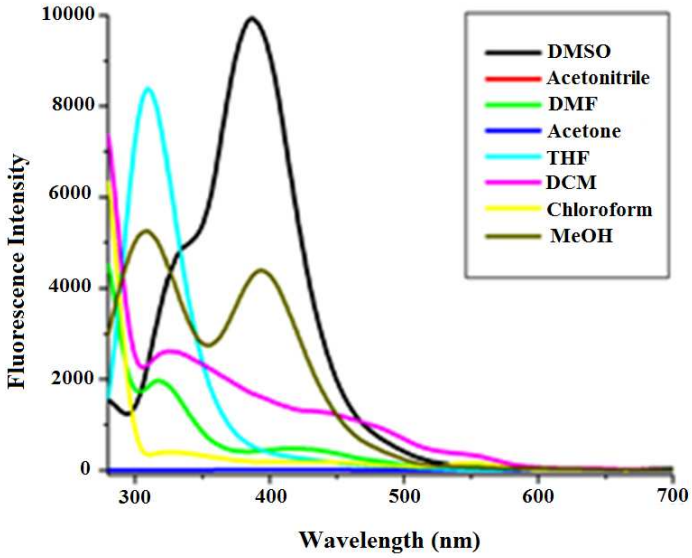

(b)

Figure 7: Fluorescence spectra for 10^{-5} M ligand (a) and complex (b) excitation at 280 nm.

The lowest polarity of the solvent may be the reason for this behaviour, therefore, the change in emission of the ligand might have occurred because of some sort of structural change in THF which dictates such behaviour. Hence, it can be concluded that the shape of the emission spectra depend neither on the concentration of the solutions, nor on the polarity of solvent. The emission spectra of solutions of the manganese (II) complex of 10^{-4}, 10^{-5} and 10^{-6} M also exhibit same pattern as in the case of free ligand, when excited at 280 nm (S1. (b)). The complex has been found to exhibit strong fluorescence emission in different solvents of various polarities, compared to free Schiff base (Figure 8(a), (b)), which may be due to increased structural rigidity and for the enhanced metal-ligand interaction[48-49] in the complex. The complex [Mn^{II} (DEMP) (NCS) (H_2O)] exhibits efficient fluorescence emission with good quantum yield of Φ_f = 0.022 which was only 0.007 in free Schiff base. The quantum yields were determined using the equation: [50]

$$Q_x = Q_s \times \left(\frac{F_x}{F_s}\right) \times \left(\frac{A_s}{A_x}\right) \times \left(\frac{\eta_x^2}{\eta_s^2}\right)$$

Where Q_x and Q_s are the quantum yield of the experimental substance and quantum yield of the standard respectively, F_x, F_s are the fluorescence area of the substance and the standard, A_s and A_x are the absorbance of the substance and the standard and η_x, η_s are the refractive indices of the substance and the standard respectively. The complex molecule is capable of harvesting the entire range of solar radiation falling on earth, and can absorb light of a wide range of wavelengths to be as close as possible to the natural photosynthetic light harvesting pigments. Hence, the present complex is having the potentiality of being used as an integral part of the artificial photosynthetic apparatus whereby it can serve a substitute for the natural photosynthetic light harvesting pigment.

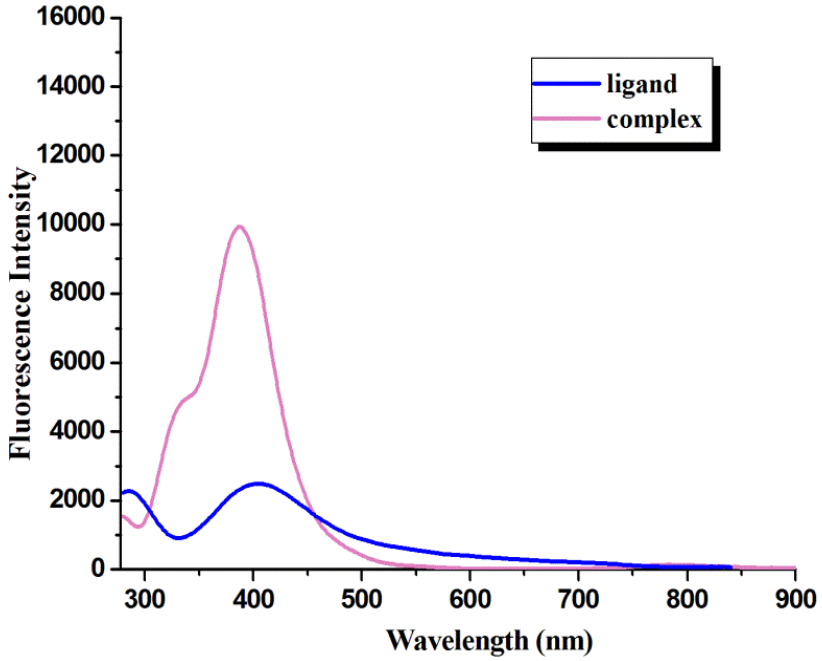

(a)

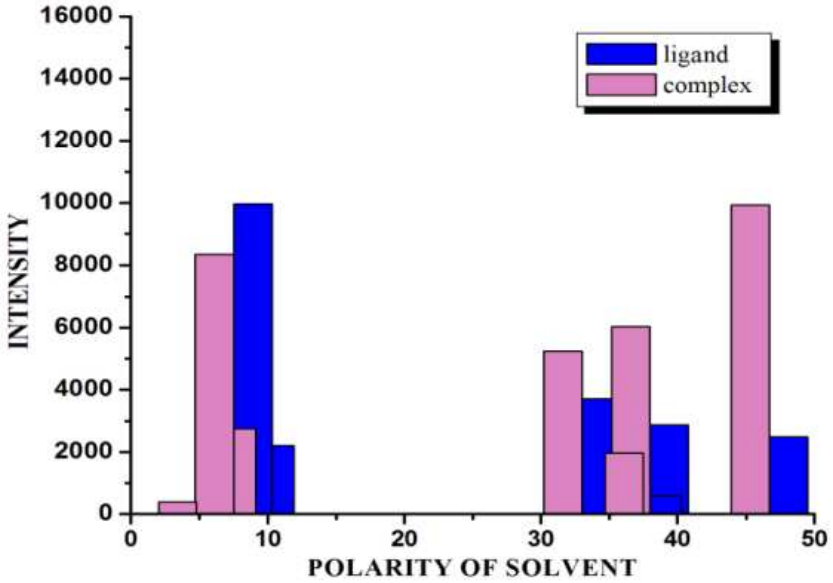

(b)

Figure 8: (a) Emission spectra of ligand and complex at room temperature (λ_{ex} = 280 nm) in DMSO (10^{-5} M). (b) Relative intensities of ligand and complex with respect to polarity of the solvents.

From the lifetime measurements[51] of both the ligand and the complex, it is also evident that the complex has shorter lifetime of fluorescence decay than the ligand and the lifetime increases with increasing polarity of the solvents (Figure 9, Table 6a, 6b.) both for the complex as well as for the ligand. Ligand exhibits higher lifetime in more polar solvents than the complex, so either there is a possibility of the involvement of the ligand in different excited state reactions like internal conversion and inter system crossings or the more polar excited state of the ligand get more stabilized in polar solvents and reside longer, exhibiting higher lifetime.

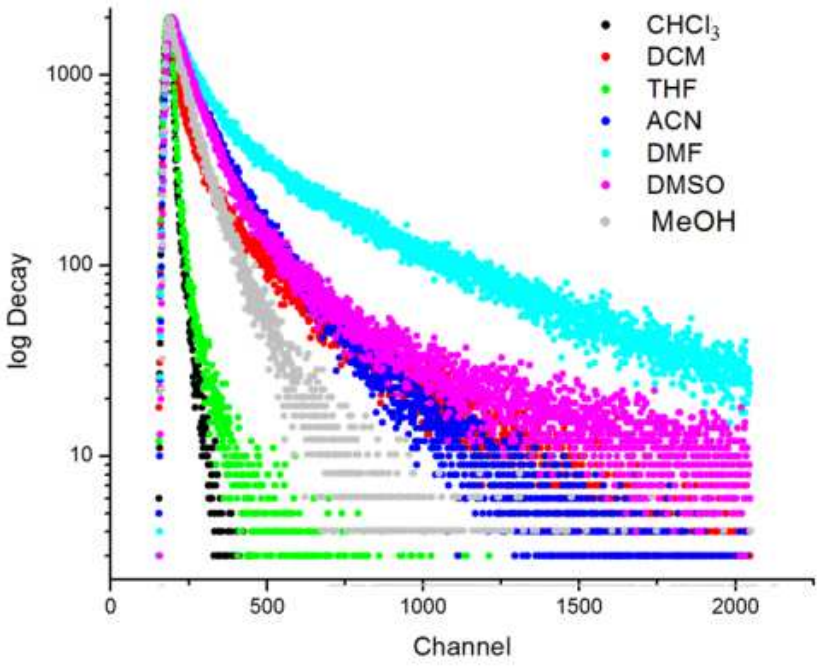

(a)

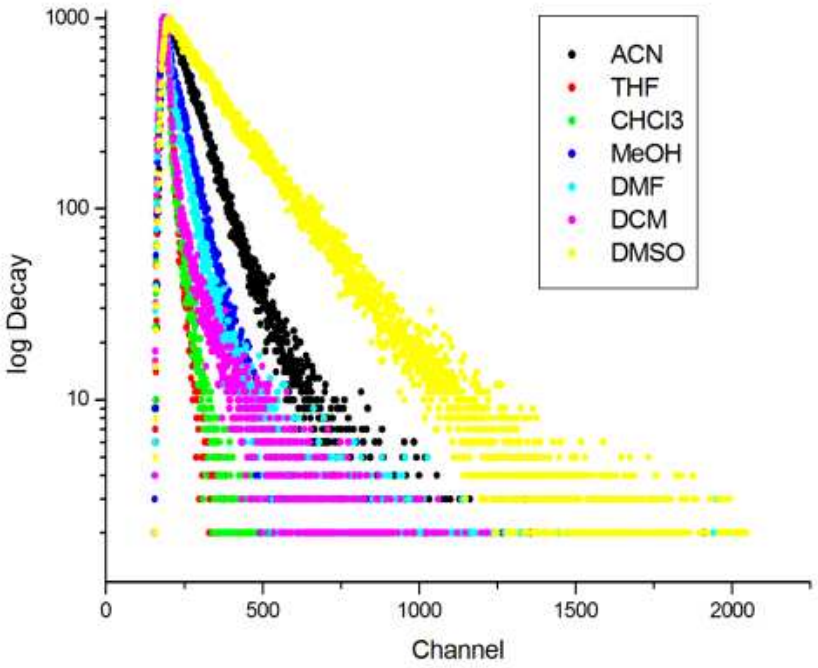

(b)

Figure 9: Fluorescence lifetime spectra for (a) ligand and (b) complex in various solvents for 10^{-5} M at 280 nm excitation wavelength.

Table 6(a): Lifetime values of fluorescence decay for the ligand in 10^{-5} M at λ_{ex} = 280 nm.

Solvents	Lifetime (ns)		Amplitude		
	τ_1	τ_2	A_1	A_2	χ^2
DMSO	1.98	7.69	0.902	0.098	1.069
DMF	2.00	12.0	0.738	0.262	1.066
Acetonitrile	2.11	5.00	0.823	0.176	1.046
MeOH	1.654	2.530	0.7247	0.2753	1.13
DCM	0.93	6.94	0.834	0.166	1.105
THF	0.11	2.00	0.974	0.026	1.006
Chloroform	0.12	1.0	0.997	0.003	1.066

Table 6(b): Lifetime values of fluorescence decay for the complex in 10^{-5} M at λ_{ex} = 280 nm.

Solvents	Lifetime (ns)		Amplitude		
	τ_1	τ_2	A_1	A_2	χ^2
DMSO	5.248	-	1.303	-	1.212
DMF	1.061	3.124	0.930	0.068	1.209
Acetonitrile	2.199	5.72	0.950	0.141	1.103
MeOH	0.0758	1.764	0.980	0.011	1.028
DCM	0.435	2.692	0.950	0.050	1.125
THF	0.142	1.177	0.990	0.012	0.873
Chloroform	0.131	1.209	0.980	0.017	1.029

Table 7: Stokes shift in nm for the complex and the ligand (DEMP) in 10^{-4} M, 10^{-5} M and 10^{-6} M solutions of various polar solvents.

Solvents	Complex 10^{-4} M (nm)	Ligand 10^{-4} M (nm)	Complex 10^{-5} M (nm)	Ligand 10^{-4} M (nm)	Complex 10^{-6} M (nm)	Ligand 10^{-6} M (nm)
DMSO	130	49	124	83	78	82
DMF	141	68	115	71	65	69
Acetonitrile	41	147	30	82	101	82
MeOH	157	49	55	48	46	48
Acetone	84	53	87	63	71	69
DCM	37	258	37	83	30	77
THF	37	44	21	40	21	69
Chloroform	27	185	22	84	27	80

To observe the solvent effect, we calculated the Stokes shifts (Table 7.) and plotted them against the polarity of the solvents (Figure 10). The Stokes' shift is seen to increase in most of the cases with an increase in the polarity of the solvent, which may be interpreted in accordance with an assumption that the complex exists in a less polar structure in less polar solvents and shows more polarity in higher polar solvents.[52]

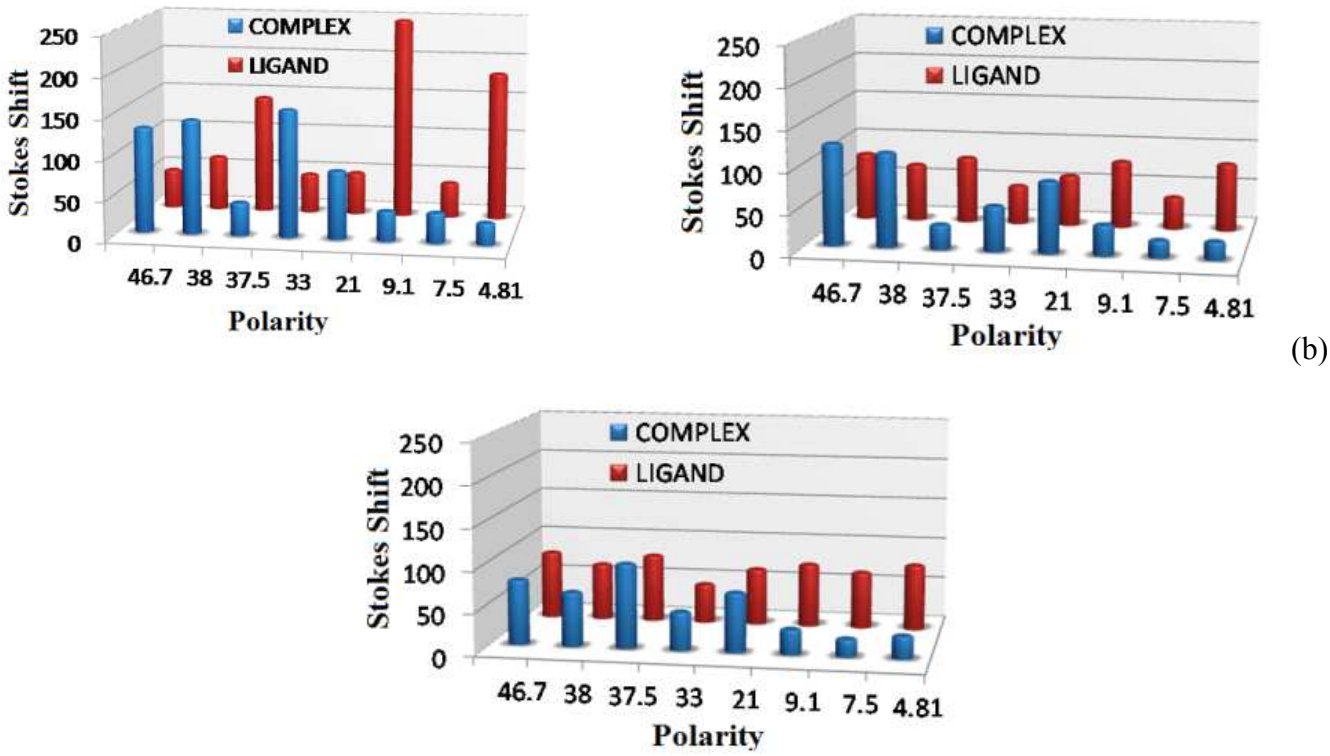

Figure 10: Stokes shift in (a) 10^{-4} M, (b) 10^{-5} M and (c) 10^{-6} M solutions of ligand (DEMP) and complex at different polarity of solvents.

Experimental

Materials

Salicylaldehyde, 2-diethylaminoethylamine, and hydroxylamine hydrochloride were obtained from Merck (India). Potassium permanganate was procured from Rankem and ammonium thiocyanate was obtained from SRL India. Solvents were purified by standard procedures[53], wherever necessary.

Physical Measurements

The IR spectra were taken as KBr discs at room temperature on a Perkin Elmer RFX-I IR spectrophotometer. UV-vis spectra (200–800 nm) were recorded at room temperature with a Perkin Elmer Lambda 25 UV-vis spectrometer against appropriate reagent blank. EPR spectra were obtained on a JEOL

– JES FA200 ESR spectrometer in solid state at 298 K. Magnetic susceptibility measurements were made using a Magway MSB MKI Magnetic susceptibility balance (Sherwood Scientific Ltd, Cambridge, England) at 298 K. Data were corrected for diamagnetic contributions using Pascal's constants. TGA study was done by Perkin Elmer - Pyris Diamond TG/DTA instrument. NMR spectral measurements were carried out in CD_3Cl solution at ambient temperature. The chemical shift was referenced to tetramethylsilane (TMS) from Bruker 300 MHz NMR spectrometer and the mass spectral analyses were done in methanol solvent from Waters Xevo® G2 QTof.

Synthesis of [Mn^{II}(DEMP)(NCS)(H_2O)]

Synthesis of Schiff base (DEMP). A 5 ml methanolic solution of salicylaldehyde (5mmol) and 2-diethylaminoethylamine (5mmol) were refluxed with continuous stirring for one and half hours. An orange solution was produced, from which the orange solid was obtained (Figure 11), after drying at 4ºC. Yield: 77%. IR (KBr, cm^{-1}): 1621 [υ (C=N)], 1542 [υ (C-O)], 3418 [υ (O-H)]. UV-vis in MeOH [λ_{max} nm (ε $M^{-1}cm^{-1}$): 253 nm (6015), 275 (5147), 312 (2108), 405 (302)]. ESI-MS (+) in MeOH: m/z (relative intensity) 221.16 [M^+, 100] (S 3.). ^{1}H NMR (300 MHz, $CDCl_3$, δ ppm): 7.46-6.78 (4H, m, aromatic protons), 8.61 (1H, s, from Ph-OH). ^{13}C NMR (75 MHz, $CDCI_3$, δ ppm): 170.28, 161.33, 136.97, 133.45, 132.13, 117.62, 117.0, 77.43, 76.58, 50.67, 30.87.

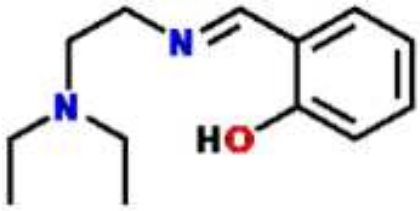

Figure 11: 2-((2-(diethylamino)ethylimino)methyl)phenol (**DEMP)**

Synthesis of complex. To 3 ml aqueous solution of potassium permanganate (5mM, 0.79g), 2ml aqueous solution of $NH_2OH.HCl$ (25mmol, 1.74g) was added and stirred for 45 minutes. Then, ammonium thiocyanate (25mmol, 1.90g) solution was added dropwise and stirred for another 30 minutes. Thereafter, 2 ml methanolic solution of 5 mmol DEMP ligand was added to the resultant solution with continuous stirring for 1 hour (Scheme 1).

Scheme 1:

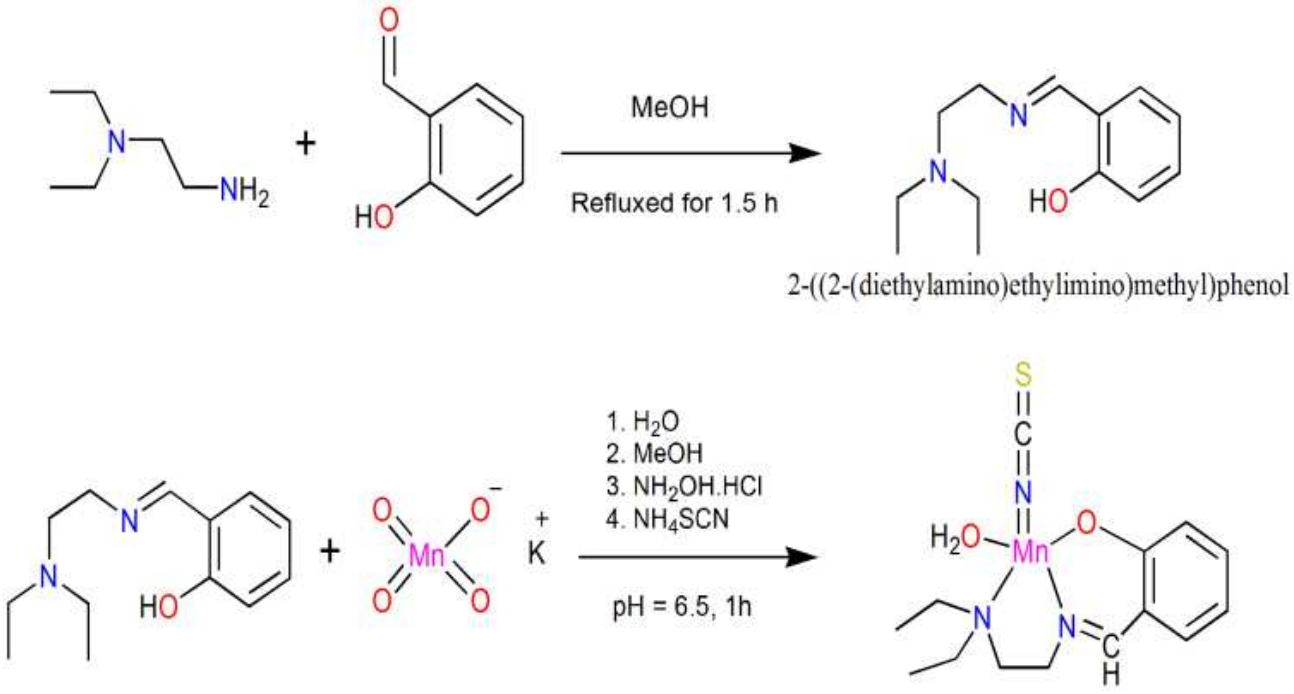

The resulting solution on standing at room temperature produced brown micro-crystalline solid after 15 days. Yield: 76%. IR (KBr, cm^{-1}): 1618.91[υ(C=N)], 2054.34 [υ (CNS)], 800.33 [υ (CS)], 3386.87 [υ (Mn-O)]. ESI-MS (+) in MeCN: m/z (relative intensity) 373.11 [M^+ + Na]. UV-vis in DCM [λ_{max} nm (ε $M^{-1}cm^{-1}$): 298 (7583), 254 (14742), 632 (3529)] (S 4). ^{1}H NMR (300 MHz, $CDCl_3$, δ ppm): 7.40-6.33 (4H, m, aromatic protons). ^{13}C NMR (75 MHz, $CDCI_3$, δ ppm): 206.948, 131.34, 130.79, 119.6, 116.78, 116.30, 77.61, 77.46, 30.91.The compound is soluble in organic solvents like methanol, acetonitrile,

chloroform, acetone, N,N-dimethyl formamide (DMF), dimethyl sulfoxide (DMSO) and tetrahydrofuran (THF) and behaves like a non-electrolyte. Despite multiple attempts, diffractable grade suitable single crystals could not be obtained.

Computational details

Ground state electronic structure calculations in methanol solution of both the ligand and complex have been carried out using DFT[54] method associated with the conductor-like polarisable continuum model (CPCM).[55-57] Becke's hybrid function[58] with the Lee-Yang-Parr (LYP) correlation function[59] was used through the study. The geometry of the ligand and complex was fully optimized without any symmetry constraints. On the basis of the optimized ground state geometry, the absorption spectral properties in methanol (CH_3OH) media were calculated by time-dependent density functional theory (TDDFT)[60-62] approach associated with the conductor-like polarisable continuum model (CPCM).[55-57] We computed the lowest 20 singlet – singlet transition and results of the TD calculations were qualitatively very similar. The TDDFT approach had been demonstrated to be reliable for calculating spectral properties of many transition metal complexes.[63-66] Due to the presence of electronic correlation in the TDDFT (B3LYP) method it can yield more accurate electronic excitation energies. Hence TDDFT had been shown to provide a reasonable spectral feature for our complex of investigation.

We have run the Gaussian for geometry optimization of complex in ground state with three different basis sets namely 6-31G, 6-311G and 6-31++G(d,p) under B3LYP. For Mn atom, we used 6-31G + G(d,p), 6-311G+ G(d,p), 6-31+ +G(d,p), for H atoms we put 6-31G,6-311G, 6-31G basis set; for C, N and O atoms we employed 6-31G,6-311G, 6-31G and for S atom we adopt 6-31G + G(d,p), 6-311G + G(d,p), 6-31+ +G(d,p) as basis set under B3LYP and compared the results, which did not show any significant change in geometrical parameters. We have used 6-31G/B3LYP basis set for ligand optimization in ground state. All the calculations were performed with the Gaussian 09W software

package.[67] GaussSum 2.1 program[68] was used to calculate the molecular orbital contributions from groups or atoms.

Fluorescence spectral study

The fluorescence spectra were measured on Elico SL 174 spectrofluorimeter following standard methods[69-70] using the excitation wavelength of 280 nm and the emission was recorded from 280 nm to 900 nm. The fluorescence intensities of the ligand and the complex were monitored in different solvents like tetrahydrofuran (THF), N,N-dimethylformamide (DMF), dimethylsulfoxde (DMSO), dichloromethane (DCM), chloroform ($CHCl_3$), acetone, acetonitrile and methanol as a function of concentration (10^{-4}, 10^{-5}, and 10^{-6} M) to observe the effects of the polarity on the photophysical activity of the complex and the ligand. The lifetimes were measured on Horiba Jobin Yvon single photon counter instrument.

Conclusions

A new [Mn^{II}(DEMP)(NCS)(H_2O)] complex has been designed and synthesized with the aim of developing a new light harvesting agent. The ability of the metal complex to absorb light over a wide region, from 200 nm to 850 nm, allows it to cover almost entirely the range of the sunlight falling on earth. The longer life times and strong fluorescence make the complex a suitable candidate for the development of new light harvesting device as well as a photoactive material.

Acknowledgements

DG is thankful to UGC-BSR for providing JRF. Authors are thankful to UGC, New Delhi for financial support in the form of Major Research Project [Sanction no.F.NO. 39-706/2010(SR)] to KKM. Financial

support from DST FIST for the EPR equipment to the Department of Chemistry, Jadavpur University is also acknowledged.

References

1 C. Andreini, I. Bertini, G. Cavallaro, G. L. Holliday and J. M. Thornton, *J. Biol. Inorg. Chem.*, 2008, 13, 1205-1218.

2 J. Roth, S. Ponzoni and M. Aschner. "Chapter 6 Manganese Homeostasis and Transport", 2013. In Banci, Lucia (Ed.). *Metallomics and the Cell*. Metal Ions in Life Sciences 12. Springer.

3 W.F. Beyer Jr. and I. Fridovich, *Biochemistry*, 1985, 24, 6460-6467.

4 S. Kamarajugadda, Q. Cai, H. Chen, S. Nayak, J. Zhu, M. He, Y. Jin, Y. Zhang, L. Ai, S.S. Martin, M. Tan and J. Lu, *Cell Death Dis.*, 2013, 4, 504.

5 S. Leitch, M. Feng, S. Muend, L. T. Braiterman, A. L. Hubbard and R. Rao, *Biometals*, 2011, 24, 159-170.

6 Z. Liu, S. Li, Y. Cai, A. Wang, Q. He, C. Zheng, T. Zhao, X. Ding and X. Zhou, *Free Radical Bio. Med.*, 2012, 53, 44-50.

7 R. M. Fronko, J. E. Penner-Hahn and C. J. Bender, *J. Am. Chem. Soc.*, 1988, 110, 7554-7555.

8 A. R. Cyr, K. E. Brown, M. L. McCormick, M. C. Coleman, A. J. Case, G. S. Watts, B. W. Futscher, D. R. Spitz and F. E. Domann, *Redox Biology*, 2013, 1, 172-177.

9 A. Ramachandran, M. Lebofsky, S. A. Weinman and H. Jaeschke, *Toxicol. Appl. Pharmacol.*, 2011, 251, 226-233.

10 R. Radmer and G. Cheniae, Primary Processes of Photosynthesis, in: J. Barber (Ed.), Topics Photosynth., Elsevier, Amsterdam, New York 1977, 303-348.

11 S. Shcolnick and N. Keren, *Plant Physiol.*, 2006, 141, 805-810.

12 B. A. Diner and P. Joliot, *Encycl. Plant Physiol.*, 1977, 5, 187-205.

13 A. Pirson , *Z. Bot.*, 1937, 31, 193-267.

14 E. Kessler, W. Arthur and J. E. Brugger, *Arch. Biochem. Biophys.*, 1957, 71, 326-335.

15 Y. Umena, K. Kawakami, J. R. Shen and N. Kamiya, *Nature*, 2011, 473, 55-60.

16 A. Grundmeier and H. Dau, *Biochim. Biophys. Acta*, 2012, 1817, 88-105.

17 G. M. Cheniae and I. F. Martin, *Biochim. Biophys. Acta*, 1970, 197, 219-239.

18 M. M. Najafpour, *J. Photochem. Photobiol. B: Biology*, 2011, 104, 111-117.

19 J. S. Kanady, E. Y. Tsui, M. W. Day and T. Agapie, *Science*, 2011, 333, 733-736.

20 G. Christou, *Acc. Chem. Res.*, 1989, 22, 328-335.

21 R. J. Debus, *Biochim. Biophys. Acta*, 1992, 1102, 269-390.

22 G. Renger, in: J. Barber Ed., Topics in Photosynthesis, the Photosystems: *Structure, Function and Molecular Biology*. Elsevier, Amsterdam, 1992, 45.

23 T. M. Bicker and D. F. Ghanotakis, in: D. R. Ort and C. F. Yocum Eds. Oxygenic Photosynthesis: The Light Reactions, Kluwer Academic, Dordrecht, 1996, 113.

24 A. Harriman, *Coord. Chem. Rev.*, 1979, 28, 147-175.

25 K. Sauer and V. K. Yachandra, *Biochim. Biophys. Acta*, 2004, 1655, 140-148.

26 H. Isobe, M. Shoji, K. Koizumi, Y. Kitagawa, S. Yamanaka, S. Kuramitsu and K. Yamaguchi, *Polyhedron*, 2005, 24, 2767-2777.

27 K. Yamaguchi, S. Yamanaka, H. Isobe, M. Shoji, K. Koizumi, Y. Kitagawa, T. Kawakami and M. Okumura, *Polyhedron*, 2007, 26, 2216-2224.

28 P. Kurz, G. Berggren, M. F. Anderlund and S. Styring, *Dalton Trans.*, 2007, 38, 4258-4261.

29 K. Wieghardt, *Angew. Chem. Int. Ed. Engl.*, 1989, 28, 1153-1172.

30 M. M. Najafpour, T. Ehrenberg, M. Wiechen and P. Kurz, *Angew. Chem. Int. Ed.*, 2010, 49, 2233-2237.

31 A. K. Poulsen, A. Rompel and C. J. McKenzie, *Angew. Chem. Int. Ed.*, 2005, 44, 6916-6920.

32 V. L. Pecoraro, M. J. Baldwin and A. Gelasco, *Chem. Rev.*, 1994, 94, 807-826.

33 L. Sun, L. Hammarström, B. Åkermark and S. Styring, *Chem. Soc. Rev.*, 2001, 30, 36-49.

34 A. Magnuson, M. Anderlund, O. Johansson, P. Lindblad, R. Lomoth, T. Polivka, S. Ott, K. Stensjö, S. Styring, V. Sundström and L. Hammarström, *Acc. Chem. Res.*, 2009, 42, 1899-1909.

35 M. Yagi and K. Narita, *J. Am. Chem. Soc.*, 2004, 126, 8084-8085.

36 M. Hakala, I. Tuominen, M. Keranen, T. Tyystjarvi and E. Tyystjarvi, *Biochim. Biophys. Acta*, 2005, 1706, 68-80.

37 R. Brimblecombe, A. Koo, G. C. Dismukes, G. F. Swiegers and L. Spiccia, *J. Am. Chem. Soc.*, 2010, 132, 2892-2894.

38 R. Croce and H. van Amerongen, *J. Photochem. Photobiol. B: Biology*, 2011, 104, 142-153.

39 S. Belaid, A. Landreau, S. Djebbar, O. Benali-Baitich, G. Bouet and J. -P. Bouchara, *J. Inorg. Biochem.*, 2008, 102, 63-69.

40 G. H. Jeffery, J. Bassett, J. Mendham and R. C. Denny Addison, Vogel's Text Book of Quantitative Chemical Analysis, Wesley Longman Limited, UK, 5th edn, 1989.

41 R. Biswas, M. G. B. Drew, C. Estarellas, A. Frontera and A. Ghosh, *Eur. J. Inorg. Chem.*, 2011, 2011, 2558-2566.

42 S. Naiya, M. G. B. Drew, C. Diaz, J. Ribas and A. Ghosh, *Eur. J. Inorg. Chem.*, 2011, 2011, 4993-4999.

43 M. J. Frisch, Gaussian 09, Revision B.01, Gaussian, Inc., Wallingford CT, 2010.

44 J. Delaunay and R. P. Hugel, *Inorg. Chem.*, 1986, 25, 3957-3961.

45 R. J. H. Clark and C. S. Williams, *Spectrochim Acta*, 1966, 22, 1081-1090.

46 B. Mabad, P. Cassoux, J. P. Tuchagues and D. N. Hendrickson, *Inorg. Chem.*, 1986, 25, 1420-1431.

47 C. Hureau, E. Anxolabèhère-Mallart, M. Nierlich, F. Gonnet, E. Rivière and G. Blondin, *Eur. J. Inorg. Chem.*, 2002, 2710-2719.

48 L. Prodi, F. Bolletta, M. Montalti and N. Zaccheroni, *Coord. Chem. Rev.*, 2000, 205, 59-83.

49 L. A. Cabell, M. D. Best, J. J. Lavigne, S. E. Schneider, D. M. Perreault, M.-K. Monahan and E. V. Anslyn, *J. Chem. Soc.*, *Perkin Trans.*, 2001, 2, 315-323.

50 S. F. Forgues and D. Lavabre, *J. Chem. Educ.*, 1999**,** 76, 1260-1264.

51 M. Sarkar, S. S. Paul and K. K. Mukherjea, *J. Lumin.*, 2013, 142, 220-230.

52 A. K. Satpati, S. Senthilkumar, M. Kumbhakar, S. Nath, D. K. Maity and H. Pal, *Photochem. Photobiol.*, 2005, 81, 270-278.

53 S. Mukherjee, J. A. Stullb, J. Yanoc, T. C. Stamatatosa, K. Pringouria, T. A. Stichb, K. A. Abbouda, R. David Brittb, V. K. Yachandrac and G. Christoua, *PNAS(Proceedings of the National Academy of Science)*, 2012, 109, 2257-2262.

54 R. G. Parr and W. Yang, *Density Functional Theory of Atoms and Molecules*, Oxford University Press, Oxford, 1989.

55 V. Barone and M. Cossi, *J. Phys. Chem. A*, 1998, 102, 1995-2001.

56 M. Cossi and V. Barone, *J. Chem. Phys.*, 2001, 115, 4708-4717.

57 M. Cossi, N. Rega, G. Scalmani and V. Barone, *J. Comp. Chem.*, 2003, 24, 669-681.

58 A. D. Becke, *J. Chem. Phys.*, 1993, 98, 5648-5652.

59 C. Lee, W. Yang and R. G. Parr, *Phys. Rev. B*, 1988, 37, 785-789.

60 M. E. Casida, C. Jamorski, K. C. Casida and D. R. Salahub, *J. Chem. Phys.*, 1998, 108, 4439-4449.

61 R. E. Stratmann, G. E. Scuseria and M. J. Frisch, *J. Chem. Phys.*, 1998, 109, 8218-8224.

62 R. Bauernschmitt and R. Ahlrichs, *Chem. Phys. Lett.*, 1996, 256, 454-464.

63 T. Liu, H.-X. Zhang and B.-H. Xia, *J. Phys. Chem. A*, 2007, 111, 8724-8730.

64 X. P. Zhou, H.-X. Zhang, Q.-J. Pan, B.-H. Xia and A.-C. Tang, *J. Phys. Chem. A*, 2005, 109, 8809-8818.

65 X. P. Zhou, A.-M. Ren and J.-K. Feng, *J. Organomet. Chem.*, 2005, 690, 338-347.

66 A. Albertino, C. Garino, S. Ghiani, R. Gobetto, C. Nervi, L. Salassa, E. Rosenverg, A. Sharmin, G. Viscardi, R. Buscaino, G. Cross and M. Milanesio, *J. Organomet. Chem.*, 2007, 692, 1377-1391.

67 M. J. Frisch, G. W. Trucks, H. B. Schlegel, G. E. Scuseria, M. A. Robb, J. R. Cheeseman, G. Scalmani, V. Barone, B. Mennucci, G. A. Petersson, H. Nakatsuji, M. Caricato, X. Li, H. P. Hratchian, A. F. Izmaylov, J. Bloino, G. Zheng, J. L. Sonnenberg, M. Hada, M. Ehara, K. Toyota, R. Fukuda, J. Hasegawa, M. Ishida, T. Nakajima, Y. Honda, O. Kitao, H. Nakai, T. Vreven, J. A. Montgomery Jr., J. E. Peralta, F. Ogliaro, M. Bearpark, J. J. Heyd, E. Brothers, K. N. Kudin, V. N. Staroverov, R. Kobayashi, J. Normand, K. Raghavachari, A. Rendell, J. C. Burant, S. S. Iyengar, J. Tomasi, M. Cossi, N. Rega, J. M. Millam, M. Klene, J. E. Knox, J. B. Cross, V. Bakken, C. Adamo, J. Jaramillo, R. Gomperts, R. E. Stratmann, O. Yazyev, A. J. Austin, R. Cammi, C. Pomelli, J. W. Ochterski, R. L. Martin, K. Morokuma, V. G. Zakrzewski, G. A. Voth, P. Salvador, J. J. Dannenberg, S. Dapprich, A. D. Daniels, Ö. Farkas, J. B. Foresman, J. V. Ortiz, J. Cioslowski and D. J. Fox, Gaussian 09, (Revision A.1), Gaussian, Inc., Wallingford, CT, 2009.

68 N. M. O'Boyle, A. L. Tenderholt, K. M. Langner, *J. Comp. Chem.*, 2008, 29, 839-845.

69 S. S. Paul, M. Selim, A. Saha and K. K. Mukherjea, *Dalton Trans.*, 2014, 43, 2835-2848.

70 S. Patra, S. Chatterjee, T. K. Si and K.K.Mukherjea, *Dalton Trans.*, 2013, 42, 13425-13435.